



RESEARCH ARTICLE

A radiomics model enables prediction venous sinus invasion in meningioma

Limei Wang^{1,†}, Yuntai Cao^{2,†}, Guojin Zhang^{3,†}, Dandan Sun¹, Wusheng Zhou¹, Wenyi Li¹, Junlin Zhou^{4,5}, Kuntao Chen¹  & Jing Zhang¹ 

¹Department of Radiology, The Fifth Affiliated Hospital of Zunyi Medical University, Zhuhai, China

²Department of Radiology, Affiliated Hospital of Qinghai University, Xining, China

³Department of Radiology, Sichuan Provincial People's Hospital, University of Electronic Science and Technology of China, Chengdu, China

⁴Department of Radiology, Lanzhou University Second Hospital, Lanzhou, China

⁵Key Laboratory of Medical Imaging of Gansu Province, Lanzhou, China

Correspondence

Junlin Zhou, Department of Radiology, Lanzhou University Second Hospital, Cuiyingmen No.82, Chengguan District, Lanzhou 730030, China. E-mail: luzjl601@163.com Kuntao Chen and Jing Zhang, Department of Radiology, The Fifth Affiliated Hospital of Zunyi Medical University, Zhufengdadao No.1439, Doumen District, Zhuhai 5191, China. Tel: 86-0756-6275796; E-mail: chenkunt2021@163.com and zymu2022@163.com; zhangj18@lzu.edu.cn

Received: 13 March 2023; Revised: 19 April 2023; Accepted: 10 May 2023

Annals of Clinical and Translational Neurology 2023; 10(8): 1284–1295

doi: 10.1002/acn3.51797

[†]The first three authors are co-first authors who contributed equally to this work.

Abstract

Objective: Preoperative prediction of meningioma venous sinus invasion would facilitate the selection of surgical approaches and predicting the prognosis. To predict venous sinus invasion in meningiomas, we used radiomic signatures to construct a model based on preoperative contrast-enhanced T1-weighted (T1C) and T2-weighted (T2) magnetic resonance imaging. **Methods:** In total, 599 patients with pathologically confirmed meningioma were retrospectively enrolled. For each patient enrolled in this study, 1595 radiomic signatures were extracted from T1C and T2 image sequences. Pearson correlation analysis and recursive feature elimination were used to select the most relevant signatures extracted from different image sequences, and logistic regression algorithms were used to build a radiomic model for risk prediction of meningioma sinus invasion. Furthermore, a nomogram was built by incorporating clinical characteristics and radiomic signatures, and a decision curve analysis was used to evaluate the clinical utility of the nomogram. **Results:** Twenty radiomic signatures that were significantly related to venous sinus invasion were screened from 3190 radiomic signatures. Venous sinus invasion was associated with tumor position, and the clinoradiomic model that incorporated the above characteristics (20 radiomic signatures and tumor position) had the best discriminating ability. The areas under the curve for the training and validation cohorts were 0.857 (95% confidence interval [CI], 0.824–0.890) and 0.824 (95% CI, 0.752–0.8976), respectively. **Interpretation:** The clinoradiomic model had good predictive performance for venous sinus invasion in meningioma, which can aid in devising surgical strategies and predicting prognosis.

Introduction

Meningiomas originate from cells of the arachnoid cap in the brain and are the most commonly occurring benign tumors of the brain and central nervous system (CNS), constituting 37.6% of all brain tumors.¹ Meningiomas that form in the walls of the sinuses located on the dura mater are known as para-sinus meningiomas. When the growth of a para-sinus meningioma is limited by the brain tissue or skull bone, it can easily invade the adjacent sinuses,² resulting in complete or incomplete obstruction of the venous sinuses. Preoperative prediction

of meningioma sinus invasion aids in surgical planning, the choice of surgical approach for paraneoplastic meningioma varies depending on the location of the tumor and the degree of venous sinus invasion; for example, meningiomas that invade the anterior 1/3 of the superior sagittal sinus (SSS), they can be removed together with the meningioma, and postoperative reconstruction of the superior sagittal sinus is not necessary; however, meningiomas that invade the middle and posterior 2/3 of the SSS or other venous sinuses, the surgical approach is different from the above and is closely related to the degree of tumor invasion of the venous sinus. Neurosurgeons must

balance the benefits and harms of radical resection and preservation of veins.³ Yamashiro *et al.*⁴ pointed out that the presence of diploic veins in patients with SSS invasion should be noted to avoid interruptions during surgery, because they can be used as a collateral venous pathway, without SSS invasion, diploic veins, even those with high blood flow, could be sacrificed. The surgical strategy chosen may also vary for different types of sinus meningiomas and further determine the patient's postoperative treatment and prognosis.⁵ Although maximum safe resection is the main treatment modality for sinus meningiomas, many postoperative complications can still occur.^{6,7} The prognoses of venous sinus invasion and meningioma are closely related; for example, extensive resection in the sagittal region during sinus invasion of meningiomas leads to impaired venous outflow and results in high disability and mortality rates.⁸ Moreover, SSS involvement was significantly associated with a higher recurrence rate.⁹ Therefore, for sinus meningiomas, reducing the postoperative recurrence rate and postoperative complications as much as possible requires the selection of a sensible surgical plan. Therefore, preoperative accurate prediction of meningioma venous sinus invasion may help in the formulation of surgical plans, thus improving the total resection rate of paranasal meningioma. It may also improve intraoperative protection of the brain tissue, reduce intraoperative bleeding, and decrease the incidence of postoperative neurological deficits, especially when the tumor is located in a functional area. Ultimately, such predictive ability may improve the prognosis and quality of life of patients with meningioma.

The provisional diagnosis of meningioma is mainly based on magnetic resonance imaging (MRI), which shows the precise position and various extensions of meningiomas.¹⁰ However, the disadvantage of MRI is that it invites highly subjective judgment from radiologists, and the final pathological diagnosis (e.g., histological classification, grading, and molecular analysis) is determined only after surgically obtaining tumor tissue,¹¹ which is not conducive to preoperative surgical planning. Accurate preoperative prediction of meningioma sinus invasion helps the surgeon to develop an individualized treatment plan (i.e., better selection of surgical techniques and improved assessment patient prognosis), thereby improving the quality of life of patients. Currently, several imaging techniques, such as digital subtraction angiography, computed tomography venography, and MR venography, are used to preoperatively assess the status of sinus invasion. Digital subtraction angiography remains the gold standard for cerebral arteriovenous visualization owing to its superior spatial resolution and hemodynamic properties; however, it is not a commonly used for the assessment of meningioma sinus invasion, it is invasive and

expensive and is mainly used for patients with large tumor volume, rich blood supply, and those requiring preoperative embolization therapy. When evaluating sinus invasion, computed tomography venography may be readily available, however, it requires injection of an iodine contrast agent with a high radiation dose. A previous study compared the performance of 3D Fast Spin-Echo T1 Black-Blood Imaging and contrast-enhanced MR venography in predicting venous sinus invasion in meningiomas.² It focused on imaging techniques and sometimes compromised the observation due to artifacts. Sun *et al.*¹² built a deep learning model to predict meningioma sinus invasion has been reported, whereas the present study focused more on image evaluation to develop clinicoradiomic predictive models and validations. Thus, there is an urgent need for a noninvasive and quantitative method to predict meningioma sinus invasion.

Radiomics is characterized by the extraction of quantitative imaging signatures or textures to interpret histopathology and the creation of a high-dimensional dataset based on the extracted signatures that transforms visual image information into deeper quantitative signatures for tumor heterogeneity assessment.^{13,14} The use of radiomic signatures to predict brain invasion of meningiomas has been reported, which may be potentially useful for preoperative prediction of venous sinus invasion.¹⁵ Therefore, the present study aimed to develop a clinicoradiomic model to predict meningioma sinus invasion by integrating radiomic and clinical features that would provide a novel tool for the prediction of venous sinus invasion based on contrast-enhanced T1- (T1C) and T2-weighted (T2) MRI sequences. We combined the advantages of radiomics methods by extracting imaging signatures that are highly correlated with venous sinus invasion and built a more efficient multi-parameter prediction model for venous sinus invasion. Further, we validated the clinical utility of the model via an external validation dataset, and provided a new approach to investigate venous sinus invasion in meningiomas.

Methods

Population

This was a retrospective study involving patients who were pathologically diagnosed with meningioma and underwent surgical resection. Between August 2015 and April 2020, 602 patients from the Fifth Affiliated Hospital of Zunyi Medical University were selected as the training cohort. Between August 2016 and April 2020, 243 patients from the Second Hospital of Lanzhou University were selected as the external validation cohort. The diagnoses of all the patients were pathologically confirmed, and the

states of venous sinus invasion were marked within the surgical records. The detailed surgical criteria are shown in the [Supplementary Materials](#). The intraoperative neurosurgeon's description was used for diagnosing the venous sinus in this study.¹⁶ According to the degree of sinus invasion, the meningiomas were classified into 3 types¹⁶: type I, Sindou I and II, in which the tumor invades the wall of the venous sinus, the detailed criteria for type I sinus invasion are described in the [Supplementary Material](#); type II, Sindou III and IV, in which the tumor grows into the venous sinus with limited narrowing of the sinus lumen; and type III, Sindou V and VI, in which the tumor grows into the venous sinus and the sinus lumen is completely occluded. Types I-III were all included in this study. The inclusion and exclusion criteria are presented in Fig. 1. The inclusion criteria were as follows: (a) pathologically confirmed meningioma with clear pathological grading (including WHO grades 1, 2, and 3 meningiomas); (b) MRI performed within one week before surgery, including T1C and T2 sequences; (c) good image quality and absence of artifacts; and (d) availability of complete clinical baseline information. The exclusion criteria were as follows: (a) patients with a history of preoperative treatment, such as radiation therapy, chemotherapy, or surgery; (b) patients who had not undergone MRI scans, had incomplete MRI sequences, or had poor MR image quality with artifacts; (c) surgical records that did not document sinus involvement; and (d) incomplete or unclear clinical baseline information. After selection of study participants according to inclusion and exclusion criteria, a total of 599 patients with meningioma were enrolled in the study. The sample consisted of 479 cases in the training cohort (220/259 = positive/negative) and 120 cases in the validation cohort (55/65 = positive/negative), who were evaluated by surgeons for venous sinus invasion. The patient characteristics are shown in Table 1. The surgical records described the status of the tumor, including shape, blood supply, relationship to surrounding tissues, and sinus invasion status.

Ethical approval was obtained from the Fifth Affiliated Hospital of Zunyi Medical University and the Second Affiliated Hospital of Lanzhou University, and the requirement of informed consent from the participants was waived.

Image acquisitions, segmentation, and standardization

MRI was performed using the 3.0-T (Siemens Verio; Siemens Vida) and 1.5-T (Siemens Magnetom Aera; Siemens Avanto Dot) scanners from the Second Hospital of Lanzhou University and Fifth Affiliated Hospital of Zunyi

Medical University, including T1C and T2 images. For detailed parameters please consult the Supplementary Material Table S1. All patients had complete MRI scans (including T1C and T2 images). Manual layer-by-layer delineation of meningioma regions on axial T1C and T2 image regions of interest (ROI) and volumes of interest (VOI) were generated by fusing the segmented tissue of each layer image. To provide a higher degree of objectivity for the manually segmented ROI, the radiologist was unaware of each patient's operative notes on pathological diagnosis before segmentation. To ensure the accuracy and validity of the results, two radiologists independently and manually segmented the MRI images. In case of any disagreement, a third radiologist with greater clinical experience confirmed the segmentation. Conventional MRI (T1C imaging) was used to determine the size, position, and presence of tumor irregularities, necrotic/cystic changes, and heterogeneous enhancement.

Indicators derived from images, such as radiomic signatures, are sensitive to acquisition settings, reconstruction algorithms, and image processing.¹² To normalize and discretize image intensity, T1C and T2 images were processed using z-score standardization, which enabled unification of data standards and improved data comparability.

Feature extraction and selection

In this study, standardized radiomic signatures were extracted from MR data using the PyRadiomics platform (<http://www.radiomics.io/pyradiomics.html>),¹⁷ and radiomic signature extraction strictly followed the Image Biomarker Standardization Initiative guidelines.¹⁸ A total of 3190 radiomic signatures were derived from the MRI images of each patient. The T1C signatures originating from the ROI were outlined in the T1C image, and the T2 signatures originating from the ROI were outlined in the T2 image.

The T1C and T2 eigen matrices were normalized. First, the mean and standard deviation of each eigenvector were calculated. The value of each eigenvector was subtracted from the mean value and divided by the standard deviation. After the normalization process, the center and unit standard deviation of each vector were zero. Due to the high dimensionality of the extracted signature space, we used Pearson Correlation Coefficient (PCC) to compare the similarity of each signature pair. In case the PCC value of the signature pair was larger than 0.9, we removed one of the signatures. After this process, the dimensions of the signature space were reduced, and each radiomic signature was independent. Before constructing the model, Recursive Feature Elimination (RFE) was used to select the signatures. Primarily, multiple models were built repeatedly, and each time the signatures with small

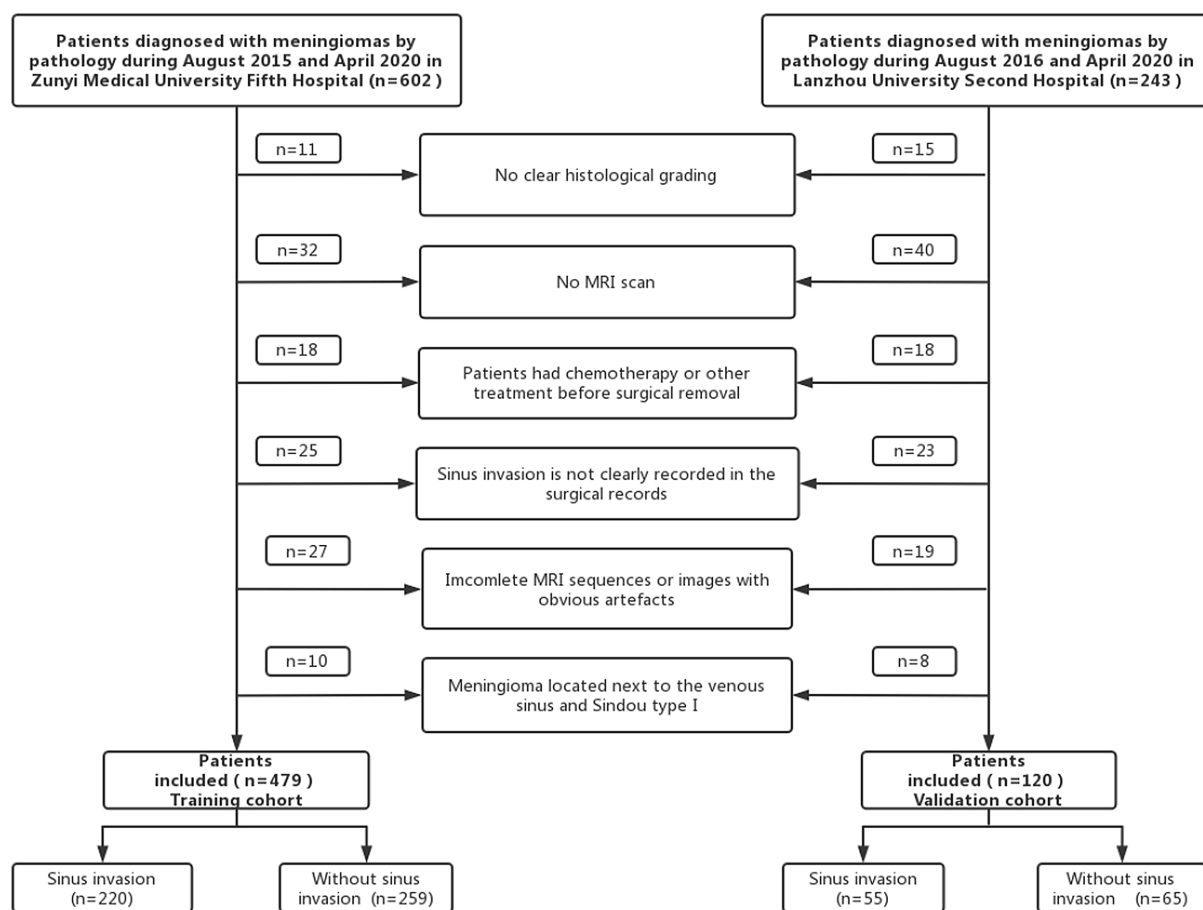


Figure 1. Inclusion and exclusion criteria.

correlation coefficients were selected and poor signatures removed. This process was repeated iteratively for the remaining signatures to obtain the smallest characteristic set and selection of signatures based on the classifier. Finally, the analysis of variance and Kruskal–Wallis test were used to select radiomic signatures that were highly correlated with venous sinus invasion (20 signatures in total). Among them, 10 T1C signatures and 10 T2 signatures were selected, including three first-order, three shape-based, and 14 texture signatures. The radiomic signatures associated with venous sinus invasion are displayed in Table 2. For example, the Neighborhood Gray-tone Difference Matrix (NGTDM) signature in T1C quantifies the sum of the differences between the gray value of a voxel and the average gray intensity of its phase voxels. The texture signature Gray-level Run-length Matrix (GLRLM) in T1C describes the spatial distribution information between neighboring voxels and the texture signature Gray-level Size Zone Matrix (GLSZM) in T2 is based on the basic principle of GLRLM to measure the distance of different voxels in the defined region. The two

texture signatures complement each other to describe the spatial distribution information of pixels/voxels.¹⁴ The correlation between these signatures shows that both sets of signatures maintained a high degree of similarity and stability in the training and validation cohorts.

For the selection of clinical risk factors, the correlation between clinical factors and meningioma sinus invasion was tested using the chi-square and Mann–Whitney U tests, with *p*-value thresholds set at 0.05. Further, signatures with *p*-values over 0.5 were excluded from the model. The chi-squared test was used to compare differences in sex, WHO grading, and tumor position. The WHO grading was a postoperative factor that was excluded from the model. The Mann–Whitney U test was used to compare differences in age (Fig. 2).

Radiomic model building

A radiomic model was created using support vector machine (SVM) and logistic regression (LR) algorithms to predict the risk of meningioma sinus invasion. The

Table 1. Clinical characteristics of patients in the training and validation cohorts.

Characteristics	Training cohort		<i>p</i> -value	Validation cohort		<i>p</i> -value
	Positive (<i>n</i> = 220)	Negative (<i>n</i> = 259)		Positive (<i>n</i> = 55)	Negative (<i>n</i> = 65)	
Sex			0.740			0.360
Male	54 (24.55%)	67 (25.87%)		13 (23.64%)	11 (16.92%)	
Female	166 (75.45%)	192 (74.13%)		42 (76.36%)	54 (83.08%)	
Age (years, mean ± SD)	51.2 ± 10.89	51.34 ± 10.95	0.977	50.82 ± 9.58	51.52 ± 9.03	0.571
Grade			0.967			0.905
Grade1	211 (95.91%)	248 (95.75%)		54 (98.18%)	64 (98.46%)	
Grade2	8 (3.63%)	10 (3.86%)		1 (1.82%)	1 (1.54%)	
Grade3	1 (0.46%)	1 (0.39%)		0	0	
Tumor position			0.002			<0.001
Parasagittal sinus	155 (70.45%)	182 (70.27%)		45 (81.82%)	40 (61.54%)	
Transverse sinus	31 (14.09%)	15 (5.79%)		5 (9.09%)	1 (1.54%)	
Sigmoid sinus	34 (15.46%)	62 (23.94%)		5 (9.09%)	24 (36.92%)	

The chi-square test was used to compare the difference in gender, WHO grade and tumor position, while the Mann–Whitney U test was used to compare the difference in age.

SD, standard deviation.

T1C	T2
t1c_log-sigma-1-mm-3D_ngtdm_Contrast	t2_exponential_firstorder_Minimum
t1c_wavelet-HLH_firstorder_Mean	t2_original_shape_Sphericity
t1c_logarithm_glcmlmc2	t2_square_gldm_DependenceVariance
t1c_wavelet-HLH_glcmlmc2	t2_wavelet-LLL_glszm_SmallAreaEmphasis
t1c_original_shape_Sphericity	t2_lbp-3D-m1_firstorder_RootMeanSquared
t1c_wavelet-LLH_glrmlm_LongRunHighGrayLevelEmphasis	t2_wavelet-HHL_glcmlm_SumSquares
t1c_original_shape_Maximum3DDiameter	t2_log-sigma-1-mm-3D_glszm_SmallAreaEmphasis
t1c_exponential_glrmlm_RunVariance	t2_log-sigma-1-mm-3D_glszm_LowGrayLevelZoneEmphasis
t1c_lbp-3D-m1_glrmlm_RunVariance	t2_wavelet-HHH_glszm_ZoneEntropy
t1c_wavelet-HLL_glszm_GrayLevelNonUniformityNormalized	t2_wavelet-LHL_glszm_SizeZoneNonUniformityNormalized

T1C, Contrast-enhanced T1-weighted magnetic resonance imaging signatures; T2, T2-weighted magnetic resonance imaging signatures.

Table 2. Radiomics features extracted from T1C and T2 that were significantly relevant with sinus invasion.

radiomic model was based on the T1C and T2 fusion signatures, which performed at the image output level (10 T1C and 10 T2 signatures), while the T1C and T2 models were developed based on the T1C and T2 signatures, respectively. We used five-fold cross-validation on the training data set to select hyper-parameters (for example, the number of signatures) of the model. The hyper-parameters were set according to the model performance (maximum area under the curve [AUC] obtained from receiver operating characteristic [ROC] analysis on the validation dataset). The calibration curves of the four models were used to compare the predictive power of the models to select the best model (Fig. 3B,C).

Establishing and validating nomogram based on radiomic characteristics and clinical risk factors

After analyzing the patients' clinical features, we found a significant correlation between the tumor position and meningioma sinus invasion ($p = 0.002$ in the training cohort and $p < 0.001$ in the validation cohort).

An SVM algorithm was used to build a model based on T1C radiomic signatures, a model based on T2 signatures, and a model based on fused T1C and T2 signatures for risk prediction of meningioma sinus invasion. The models were compared and analyzed for their ability to

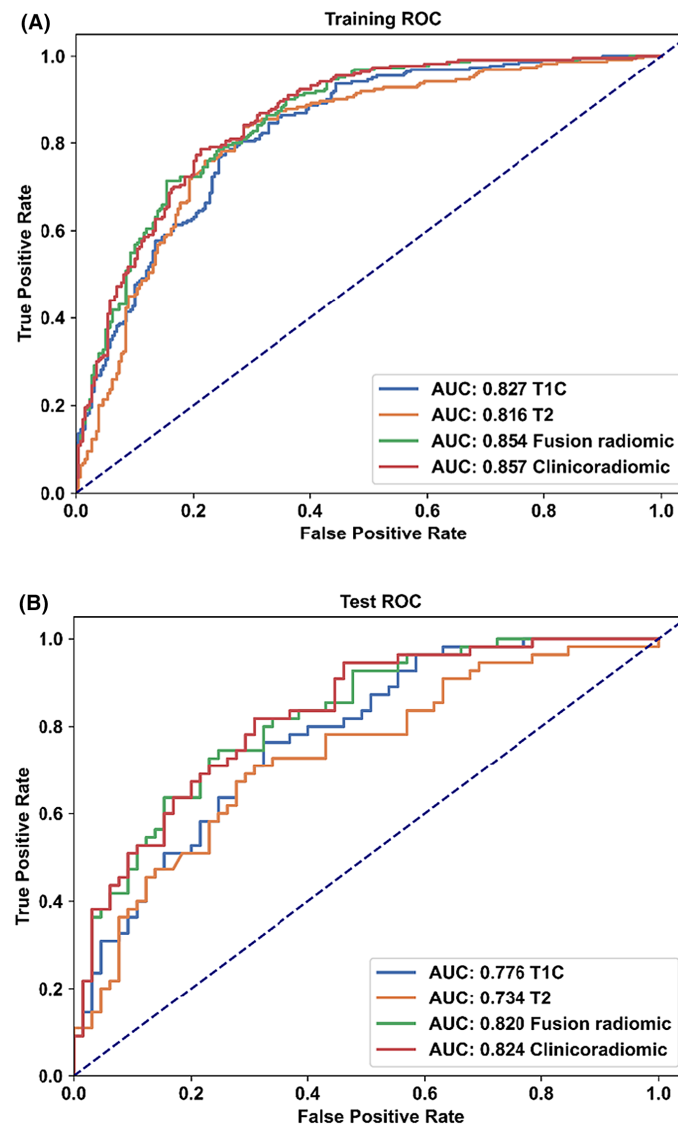


Figure 2. Comparison of the receiver operating characteristic (ROC) curves of different models. ROC curves of the different models in the training (A) and validation (B) cohort. The clinicoradiomic model demonstrated the best discriminating ability among these models, with an AUC of 0.857 in the training cohort and an AUC of 0.824 in the validation cohort.

discriminate between different models in terms of the risk of venous sinus invasion. Integrated discrimination improvement (IDI) and the DeLong test were used to select the best model. Further, IDI was conducted to quantify the performance improvement and reflect the overall improvement of the model, and a p -value < 0.05 indicated a statistically significant improvement in reclassification by comparing the T1C and T2 the models alone. Notably, the inclusion of T1C and T2 signatures improved the predictive performance of the model. After comparing the models, the best one was selected to

develop the nomogram¹⁹ that was created using the training cohort, and included radiomic signatures and clinical risk factors. It elaborated the relationship between signatures and meningioma sinus invasion, which was validated on an external validation set.

Statistical analysis

Python (version 3.7.6) and R (version 4.1.1; The R Foundation for Statistical Computing, Vienna, Austria) were used for all statistical analyses. Subtype variables including

sex, WHO grading, and tumor position were statistically analyzed using chi-square tests in the training and validation cohort. The Mann–Whitney U test was used for statistical analysis of continuous variables, and statistical descriptions are presented as mean \pm standard deviation. Generally, two-sided p -values < 0.05 were considered statistically significant.

Results

Clinical characteristics of patients with meningioma

In total, 599 patients were included in this study. We selected 479 cases in the training cohort and 120 cases in the external independent validation cohort. Table 1 shows the clinical characteristics of the patients. Four clinical variables were collected in our study, including age, sex, tumor position, and WHO grading. For clinical characteristics, tumor position differed significantly ($p = 0.002$ in the training cohort and $p < 0.001$ in the validation cohort) between patients with and without meningioma sinus invasion. Sex, WHO grading, and age were not significantly different in the two groups ($p > 0.05$).

Fusion of modalities

Overall, 1595 radiomic signatures were extracted from T1C and T2 sequences, respectively. Since MRI-derived signatures have a high dimensionality, we compared the similarity of each signature pair using PCC to reduce the dimension. We selected highly relevant and mutually independent radiomic signatures of meningioma sinus invasion using recursive feature elimination. In total, 20 of the 3190 radiomic signatures that were significantly related to meningioma sinus invasion were selected. The analysis showed that the tumor position differed significantly between patients with and without venous sinus invasion. Signatures with a p -value > 0.05 and postoperative factors (WHO grading) were excluded from the model. Thus, radiomic signatures and tumor positions were selected for the clinicoradiomic model building; the model was visualized and the nomogram was established in this study, which is shown in Fig. 3A.

After model combination, the clinicoradiomic model obtained by fusing the tumor position, three first-order signatures, three shape-based signatures, and 14 texture signatures had the best predictive ability. The AUC values of the clinicoradiomic predictive models were 0.857 (95% CI, 0.824–0.890) and 0.824 (95% CI, 0.752–0.897) for sinus invasion prediction in the training and validation cohorts, respectively. Sensitivity and specificity were 81.82% and 69.23%, respectively (Table 3).

Model comparisons

The DeLong test was used to assess the significance of the AUC values of the ROC curves, with a p -value < 0.05 indicating a statistically significant AUC value for the comparison models. The clinicoradiomic model showed the best predictive performance in the training and validation cohorts. The AUC value for the training and validation cohorts was 0.857 (95% CI, 0.824–0.890) and 0.824 (95% CI, 0.752–0.897), respectively (Table 4), and sensitivity and specificity were 81.82% and 69.23%, respectively, in the validation cohort.

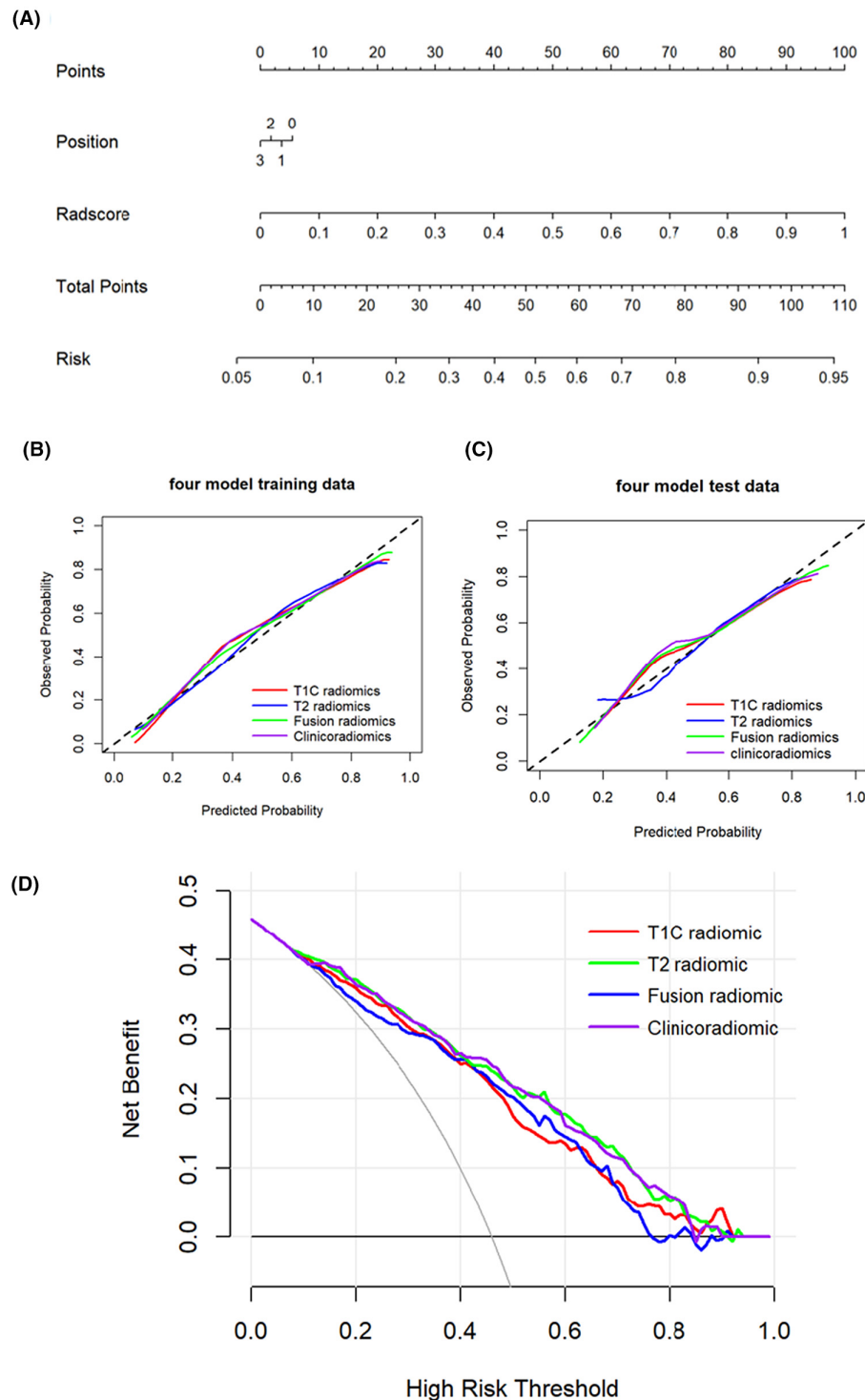
An IDI²⁰ metric was used to evaluate the incremental predictive ability of different prognostic models. The clinicoradiomic model improved by 1.57% ($p = 0.001$) and 0.43% ($p = 0.645$) as compared to the radiomic model in the training and validation cohorts, respectively. Comparisons between different models are shown in Table 5.

Clinicoradiomic nomogram performance

In addition to using AUC for quantifying the discrimination, calibration curves were applied to assess the predictive ability of the four models (Fig. 3B,C) and determine the fit superiority of the models. The result identified the best performing clinicoradiomic model and defined the radiomic nomogram. The decision curve analysis (DCA) was used to quantify the net benefit at different threshold probabilities in this study,²¹ the clinicoradiomic model had the highest value of use when the threshold value was 0.2 to 0.8. Accordingly, the nomogram was assessed for clinical validity. The decision curves for the four models are shown in Fig. 3D.

Discussion

The present study used MRI and large-scale data to predict the risk of venous sinus invasion in meningiomas using a clinicoradiomic model. The performance of this model was validated using discrimination, sensitivity, specificity, calibration curves, and DCA. A fused radiomic model showed a beneficial predictive performance in the training (AUC: 0.854) and validation (AUC: 0.820) cohorts. The nomogram, based on radiomic signatures and tumor position information, showed the best predictive performance. Further, the AUC values of the clinicoradiomic model were 0.857 and 0.824 in the training and validation cohorts, respectively. Sensitivity and specificity were 81.82% and 69.23%, respectively. These findings imply that clinicoradiomic models can be used to preoperatively identify venous sinus invasion in meningioma patients. Thus, this study provides a noninvasive and convenient alternative for clinicians to evaluate patients with venous sinus invasion.



Tumor position differed significantly ($p = 0.02$ in the training cohort and $p < 0.001$ in the validation cohort) between positive and negative patients. The tumor position was identified as a significant factor for venous

sinus invasion. Further, meningiomas invading the parasagittal sinus were present in 76.36% and 54.55% of the patients in the training and validation cohorts, respectively, which was consistent with the finding of

Figure 3. The Nomogram development and validation. The Nomogram development and validation. (A) Radiomic nomogram for predicting sinus status of meningiomas. The radiomics nomogram was developed in the training cohort, with the radiomic signatures and clinical signature (tumor position). (B) Calibration curve for the four models in the training cohort. (C) Calibration curve for the four models in the validation cohort. The x-axis represents the probability of sinus invasion measured using the four models, and the y-axis represents the actual rate of sinus invasion. The solid line represents the discrimination ability of the nomogram, while the diagonal dotted line represents an ideal evaluation by a perfect model. The closer the solid line and the dotted line are proposed to fit, the better the prediction accuracy of the nomogram. The calibration curve shows the calibration of a consistent column line plot between the predicted risk of sinus invasion status and pathological findings. (D) Decision curve analysis for the T1C, T2, fusion model, and clinicoradiomic model. The x-axis shows the threshold probability, and the y-axis measures the net benefit. The gray line represents all patients with sinus invasion, while the black line represents all patients without sinus invasion. The purple line represents the clinicoradiomic model.

Model	AUC (95% CI)	ACC (%)	SPE (%)	SEN (%)	NPV	PPV
T1C	0.776 (0.694–0.857)	71.67	67.69	76.36	0.772	0.667
T2	0.734 (0.644–0.824)	70.00	69.23	70.91	0.738	0.661
Combination of T1C and T2	0.820 (0.747–0.894)	75.00	75.38	74.55	0.778	0.719
Clinicoradiomic	0.824 (0.752–0.897)	75.00	69.23	81.82	0.818	0.692

Table 3. Performance of models for sinus invasion prediction in the validation cohort.

ACC, balanced accuracy; AUC, area under receiver operating characteristic curve; Clinicoradiomic, fusion of radiomic signatures and tumor position; NPV, negative predictive value; PPV, positive predictive value; SEN, sensitivity; SPE, specificity; T1C, contrast-enhanced T1-weighted imaging features; T2, T2-weighted imaging features; T1C+T2, combination of T1C and T2 features.

Table 4. Performance of models for sinus invasion prediction (AUC) in the training cohort and validation cohort.

Cohort	Model	AUC (95% AUC CI)	New model	AUC (95% AUC CI)	DeLong test (p-Value)
Training cohort	T1C ¹	0.827 (0.791–0.863)	Combination of T1C and T2 ³	0.854 (0.820–0.887)	$p^{13} = 0.063$
	T2 ²	0.816 (0.778–0.855)	Combination of T1C and T2 ³	0.854 (0.820–0.887)	$p^{23} = 0.018$
	Combination of T1C and T2 ³	0.854 (0.820–0.887)	Clinicoradiomic ⁴	0.857 (0.824–0.890)	$p^{34} = 0.237$
Validation cohort	T1C ¹	0.776 (0.694–0.857)	Combination of T1C and T2 ³	0.820 (0.747–0.894)	$p^{13} = 0.255$
	T2 ²	0.734 (0.644–0.824)	Combination of T1C and T2 ³	0.820 (0.747–0.894)	$p^{23} = 0.028$
	Combination of T1C and T2 ³	0.820 (0.747–0.894)	Clinicoradiomic ⁴	0.824 (0.752–0.897)	$p^{34} = 0.3$

Table 5. Comparison between different models in the training and validation cohort (IDI).

Cohort	Model	New model	IDI	p-Value
Training cohort	Combination of T1C and T2	Clinicoradiomic	1.57%	$p = 0.001$
	T1C	Combination of T1C and T2	5.33%	$p = 0.001$
	T2	Combination of T1C and T2	10.56%	$p < 0.000$
Validation cohort	Combination of T1C and T2	Clinicoradiomic	0.43%	$p = 0.645$
	T1C	Combination of T1C and T2	6.39%	$p = 0.120$
	T2	Combination of T1C and T2	14.87%	$p = 0.000$

IDI, integrated discriminant improvement.

other reports (42.9%–85.71%),^{22,23} this may demonstrate that parasagittal sinus meningiomas are more prone to venous sinus invasion, as these lesions are located near the SSS and there is no brain parenchyma

between the meningioma and the SSS. As reported by Mantovani and Mohammed *et al.*, the parasagittal meningioma subgroup accounts for 19.5%–45% of all intracranial meningiomas.^{24,25} Further, parasagittal and

falcine meningiomas are the second most frequently occurring intracranial meningiomas.⁶

Some studies have reported prediction of grading, differential diagnosis, and prognosis of meningiomas using radiomic signatures (e.g., T1C, T2, DWI, T1WI, T1C, and ADC mapping).^{8,26–28} Hence, we explored the radiomic signatures associated with meningioma sinus invasion. The model based on 20 signatures had the highest AUC for the training and validation cohorts. Most signatures were texture signatures of the image (14/20), which can describe tumor microstructures that are not easily identified visually, such as cellularity, heterogeneity, and peritumor edema and may be associated with tumor aggressiveness.^{27,29,30} For example, NGTDM may describe tumor heterogeneity with key signatures including coarseness, busyness, and complexity, with roughness describing the spatial rate of change of gray values and busyness describing the rapid rate of change of gray values.¹⁴ Previous studies have reported that these imaging signatures are highly correlated with brain and bone invasion in meningiomas.^{15,31} In addition, GLSZM and GLRLM—two signatures that are highly relevant in brain and bone invasion—may describe the spatial distribution of cells. Notably, GLSZM was the most relevant for bone invasion.²⁹ These correlated signatures may reveal some microscopic connections between the brain, sinus, and bone invasion that are otherwise difficult to recognize visually. The first-order signatures describe the distribution of voxel intensities within the MRI images. Shape-based signatures describe the grayscale intensity distribution in the ROI, encompassing the size and shape of the tumor region. All these imaging histological signatures are associated with cellular heterogeneity and may expose the nature of tissue invasion around meningiomas. Therefore, radiomic signatures can be used as a noninvasive method to predict preoperative meningioma sinus invasion.

A recent study used deep learning to automatically segment contoured clinical target volumes,³² quantitatively translate tumor expression at the microphysical level, and realize tumor heterogeneity visualization. In another study, we built a deep-learning radiomics analysis model to identify venous sinus invasion.¹² It is also important to assess peri-meningioma tissue invasion.¹⁵ In the present study, LR and SVM algorithms were used to build a clinicoradiomic model for the risk prediction of meningioma sinus invasion. The results showed that the combined clinicoradiomic model demonstrated a desirable performance in predicting meningioma sinus invasion by evaluating the model's discrimination, calibration, and clinical utility. A nomogram—a visualization mode of LR—incorporating radiomic signatures and clinical risk factors was established, which transformed complex regression equations into visual graphics, making the results of the model more

readable, intuitive, and understandable. Nomograms not only have a good predictive power but are also non-invasive methods that facilitate clinicians in assessing patients and developing surgical strategies preoperatively. The current research demonstrates a significant association of signatures with meningioma sinus invasion, including first-order signatures, shape heterogeneity, texture signatures, and tumor position. Further, the constructed nomogram can be used as a non-invasive, convenient, and quantitative method for preoperative prediction of venous sinus invasion in patients with meningioma.

The present study had some limitations. First, this was a retrospective study, the criterion for sinus invasion of meningiomas in this study was obtained by intraoperative assessment by the surgeons, which was subjective, especially type I, and there may be false positives or negative, leading to biased results. Second, ROIs were manually delineated by radiologists, which can be highly time- and energy-consuming. Third, in this study, satisfactory independent validation results were obtained, but in future studies, the model could be trained internally and externally in multiple centers to improve its repeatability, robustness, and generalization ability. Ultimately, T1C and T2 sequence images were selected to extract radiomic signatures, and some of the T2 boundaries were blurred and may have been biased even though they were outlined with reference to the T1C image.

Conclusions

Based on manually extracted radiomic signatures, meningioma venous sinus invasion was significantly correlated with the constructed radiomic labels. The clinicoradiomic model constructed in this study had a beneficial predictive performance for meningioma sinus invasion, provided validity to the model, and showed good predictive and generalization abilities. Clinicoradiomic models may be a potentially useful and actionable tool for predicting sinus invasion in meningiomas.

Author Contributions

Jing Zhang, Kuntao Chen, and Junlin Zhou contributed to the conception of the study; Wang Limei, Cao Yuntai, and Zhang Guojin contributed significantly to the analysis of the data and wrote the manuscript; Dandan Sun, Wusheng Zhou, and Wenyi Li helped perform the analysis with constructive discussions.

Acknowledgements

Thank individuals who contributed to the study or manuscript preparation but who do not fulfill all the criteria of

authorship. Thank you to the organizations that provided financial support: Medical Science and Technology Research Fund Project of Guangdong Province (B2022144), Science and Technology Plan Fund of Guizhou Provincial (Qiankehe Foundation-ZK [2022] General 634), Doctoral research start-up fund project of Zunyi Medical University (BS2021-03), National Natural Science Foundation of China (82260341), Science and Technology Fund Project of Guizhou Provincial Health Commission (gzwkj2021-375), The Sichuan Academy of Medical Science & Sichuan Provincial People's Hospital Research Fund (2022QN25), and Qinghai Province "Kunlun Talents High-end Innovation and Entrepreneurial Talents" Top Talent Cultivation Project ([2021] 13).

Conflict of Interest

The authors would like to declare that no potential conflicts of interest with any commercial entities relating to this study.

References

- Ostrom QT, Cioffi G, Gittleman H, et al. CBTRUS statistical report: primary brain and other central nervous system tumors diagnosed in the United States in 2012-2016. *Neuro Oncol*. 2019;21:v1-v100. doi:10.1093/neuonc/noz150
- Wang D, Lu Y, Yin B, et al. 3D fast spin-Echo T1 black-blood imaging for the preoperative detection of venous sinus invasion by meningioma: comparison with contrast-enhanced MRV. *Clin Neuroradiol*. 2019;29:65-73. doi:10.1007/s00062-017-0637-1
- Zhang N, Yang T, Hameed F, et al. Can safe and radical resection of all types of parasagittal meningiomas be achievable?—the introduction of a simplified surgical strategy. *Neurol Res*. 2021;43:259-266. doi:10.1080/01616412.2020.1847530
- Yamashiro K, Muto J, Wakako A, et al. Diploic veins as collateral venous pathways in patients with dural venous sinus invasion by meningiomas. *Acta Neurochir*. 2021;163:1687-1696. doi:10.1007/s00701-021-04777-4
- Giordan E, Sorenson TJ, Lanzino G. Optimal surgical strategy for meningiomas involving the superior sagittal sinus: a systematic review. *Neurosurg Rev*. 2020;43:525-535. doi:10.1007/s10143-018-1026-1
- Cucu AI, Turliuc MD, Costea CF, et al. Tumor recurrence in parasagittal and falxine atypical meningiomas invading the superior sagittal sinus. *Rom J Morphol Embryol*. 2020;61:385-395. doi:10.47162/RJME.61.2.08
- Niu L, Zhou X, Duan C, et al. Differentiation researches on the meningioma subtypes by radiomics from contrast-enhanced magnetic resonance imaging: a preliminary study. *World Neurosurg*. 2019;126:e646-e652. doi:10.1016/j.wneu.2019.02.109
- Zabolotny RA, Fedyanin AV, Yulchiev UA, Galkin MV, Kozlov AV. Comprehensive treatment of patients with parasagittal meningiomas. *Zh Vopr Neirokhir Im N N Burdenko*. 2019;83:121-125.
- Gomes dos Santos A, Solla DJF, Moscardi R, et al. Adjuvant radiotherapy did not reduce recurrence of World Health Organization grade I meningiomas with venous sinus involvement: a propensity score adjusted analysis and literature review. *World Neurosurg*. 2019;130:e1015-e1019.
- Sindou M, Nebbal M, Guclu B. Cavernous sinus meningiomas: imaging and surgical strategy. *Adv Tech Stand Neurosurg*. 2015;42:103-121. doi:10.1007/978-3-319-09066-5_6
- Goldbrunner R, Minniti G, Preusser M, et al. EANO guidelines for the diagnosis and treatment of meningiomas. *Lancet Oncol*. 2016;17:e383-e391. doi:10.1016/s1470-2045(16)30321-7
- Sun K, Zhang J, Liu Z, et al. A deep learning radiomics analysis for identifying sinus invasion in patients with meningioma before operation using tumor and peritumoral regions. *Eur J Radiol*. 2022;149:110187. doi:10.1016/j.ejrad.2022.110187
- Lambin P, Rios-Velazquez E, Leijenaar R, et al. Radiomics: extracting more information from medical images using advanced feature analysis. *Eur J Cancer*. 2012;48:441-446. doi:10.1016/j.ejca.2011.11.036
- Mayerhoefer ME, Materka A, Langs G, et al. Introduction to radiomics. *J Nucl Med*. 2020;61:488-495. doi:10.2967/jnumed.118.222893
- Zhang J, Yao K, Liu P, et al. A radiomics model for preoperative prediction of brain invasion in meningioma non-invasively based on MRI: a multicentre study. *EBioMedicine*. 2020;58:102933. doi:10.1016/j.ebiom.2020.102933
- Maiuri F, Donzelli R, Pagano S, Mariniello G. The management of the venous sinuses during surgery for posterior fossa meningiomas. *World Neurosurg*. 2019;125:357-363. doi:10.1016/j.wneu.2019.02.032
- van Griethuysen JJM, Fedorov A, Parmar C, et al. Computational radiomics system to decode the radiographic phenotype. *Cancer Res*. 2017;77:e104-e107. doi:10.1158/0008-5472.CAN-17-0339
- Zwanenburg A, Vallieres M, Abdalah MA, Aerts H. The image biomarker standardization initiative: standardized quantitative radiomics for high-throughput image-based phenotyping. *Radiology*. 2020;295:328-338.
- Hyder O, Marques H, Pulitano C, et al. A nomogram to predict long-term survival after resection for intrahepatic cholangiocarcinoma: an eastern and Western experience. *JAMA Surg*. 2014;149:432-438. doi:10.1001/jamasurg.2013.5168
- Pencina MJ, D'Agostino RB Sr, Demler OV. Novel metrics for evaluating improvement in discrimination: net

- reclassification and integrated discrimination improvement for normal variables and nested models. *Stat Med*. 2012;31:101-113. doi:[10.1002/sim.4348](https://doi.org/10.1002/sim.4348)
21. Vickers AJ, Holland F. Decision curve analysis to evaluate the clinical benefit of prediction models. *Spine J*. 2021;21:1643-1648. doi:[10.1016/j.spinee.2021.02.024](https://doi.org/10.1016/j.spinee.2021.02.024)
 22. Mantovani A, Di Maio S, Ferreira MJ, Sekhar LN. Management of meningiomas invading the major dural venous sinuses: operative technique, results, and potential benefit for higher grade tumors. *World Neurosurg*. 2014;82:455-467.
 23. Mohammed N, Narayan V, Patra D, Savardekar AR, Riaz M, Nanda A. Management of meningiomas involving the major venous sinuses: a single-institution experience. *World Neurosurg*. 2019;127:e179-e185.
 24. Anthofer J, Seidel-Schulz R, Proescholdt M, Brawanski A, Schebesch K-M. Meningiomas adjacent to major venous sinuses—clinical outcome and recurrence. *World Neurosurg*. 2017;104:560-566.
 25. Mathiesen T, Pettersson-Segerlind J, Kihlström L, Ulfarsson E. Meningiomas engaging major venous sinuses. *World Neurosurg*. 2014;81:116-124. doi:[10.1016/j.wneu.2013.01.095](https://doi.org/10.1016/j.wneu.2013.01.095)
 26. Yang L, Xu P, Zhang Y, et al. A deep learning radiomics model may help to improve the prediction performance of preoperative grading in meningioma. *Neuroradiology*. 2022;64:1373-1382.
 27. Zhang Y, Chen JH, Chen TY, et al. Radiomics approach for prediction of recurrence in skull base meningiomas. *Neuroradiology*. 2019;61:1355-1364.
 28. Laukamp KR, Shakirin G, Baessler B, et al. Accuracy of radiomics-based feature analysis on multiparametric magnetic resonance images for noninvasive meningioma grading. *World Neurosurg*. 2019;132:e366-e390.
 29. Yan PF, Yan L, Hu TT, et al. The potential value of preoperative MRI texture and shape analysis in grading meningiomas: a preliminary investigation. *Transl Oncol*. 2017;10:570-577.
 30. Park YW, Oh J, You SC, et al. Radiomics and machine learning may accurately predict the grade and histological subtype in meningiomas using conventional and diffusion tensor imaging. *Eur Radiol*. 2019;29:4068-4076. doi:[10.1007/s00330-018-5830-3](https://doi.org/10.1007/s00330-018-5830-3)
 31. Zhang J, Sun J, Han T, et al. Radiomic features of magnetic resonance images as novel preoperative predictive factors of bone invasion in meningiomas. *Eur J Radiol*. 2020;132:109287. doi:[10.1016/j.ejrad.2020.109287](https://doi.org/10.1016/j.ejrad.2020.109287)
 32. Zabihollahy F, Viswanathan AN, Schmidt EJ, Lee J. Fully automated segmentation of clinical target volume in cervical cancer from magnetic resonance imaging with convolutional neural network. *J Appl Clin Med Phys*. 2022;23:e13725. doi:[10.1002/acm2.13725](https://doi.org/10.1002/acm2.13725)

Supporting Information

Additional supporting information may be found online in the Supporting Information section at the end of the article.

Figure S1.
Table S1.